Energy & Environmental Science

ROYAL SOCIETY OF CHEMISTRY

PAPER

View Article Online
View Journal

Cite this: DOI: 10.1039/d0ee03567j

Solar photoelectrochemical synthesis of electrolyte-free H_2O_2 aqueous solution without needing electrical bias and H_2†

Tae Hwa Jeon, [ab] Bupmo Kim, [a] Chuhyung Kim, [a] Chuan Xia, [c] Haotian Wang, [c] Pedro J. J. Alvarez *[b] and Wonyong Choi *[a]

The conventional synthesis of hydrogen peroxide (H_2O_2) such as heterogeneous catalytic and electrochemical processes requires H_2 and O_2 as reagents, costly noble metals, and organic solvents, which are energy/waste-intensive and hazardous. An alternative method of photoelectrochemical (PEC) synthesis that needs only water and sunlight is environment-friendly but its practical application is limited due to the energy-demanding method for the separation of the synthesized H_2O_2 from the electrolytes. Herein, we demonstrated the direct synthesis of an electrolyte-free aqueous solution of pure H_2O_2 by developing a PEC system with solid polymer electrolyte (SPE) and engineered electrodes. Ruthenium catalyst-decorated TiO_2 nanorods (RuO_x/TNR: photoanode) and anthraquinone-anchored graphite rods (AQ/G: cathode) are placed in an anode compartment and a cathode compartment, respectively, while a middle compartment containing SPE is located between these compartments. Upon solar simulating irradiation (AM 1.5G, 100 mW cm^{-2}), the photoanode generates H^+ ions *via* water oxidation reaction (WOR) and the cathode generates HO_2^- ions *via* two-electron oxygen reduction reaction (ORR), while the SPE selectively transports H^+ and HO_2^- into the middle compartment to form pure H_2O_2 solution. The combined system enabled continuous H_2O_2 synthesis over 100 h even under bias-free (0.0 V of cell voltage) conditions with the production of ~80 mM H_2O_2 (electrolyte-free) and a faradaic efficiency of ~90%, which is the highest concentration of pure H_2O_2 obtained using PEC systems. This study successfully demonstrates the proof-of-concept that might enable the production of a concentrated pure (electrolyte-free) aqueous solution of H_2O_2 using sunlight, water, and dioxygen only.

Received 10th November 2020,
Accepted 15th March 2021

DOI: 10.1039/d0ee03567j

rsc.li/ees

Broader context

The current industrial production process of H_2O_2 that is energy-intensive and environmentally unsustainable has motivated the search for alternative methods for greener production. The photoelectrochemical (PEC) system is an eco-friendly method that uses sunlight, water and dioxygen only, without using H_2 gas. Herein, we develop a new PEC-based system to produce pure aqueous H_2O_2 solution free from electrolytes. The proposed system is based on a three-compartment-stack cell, which consists of a RuO_x-loaded TiO_2 nanorod photoanode, an anthraquinone-anchored cathode, and solid polymer electrolyte (SPE). Engineering of both the photoanode and cathode achieves a successful system operation under bias-free conditions with high efficiency and durability. The SPE in the middle cell that is located between the photoanode and the cathode facilitates the selective transport of H^+ and HO_2^- ions that are generated from water oxidation and oxygen reduction at the photoanode and the cathode, respectively, to produce pure (electrolyte-free) H_2O_2 solution. The overall photosynthesis process needs water and dioxygen only, without external electrical bias and H_2 gas.

[a] *Division of Environmental Science and Engineering, Pohang University of Science and Technology (POSTECH), Pohang 37673, Republic of Korea. E-mail: wchoi@postech.edu*

[b] *Department of Civil and Environmental Engineering, Rice University, Houston, TX 77005, USA*

[c] *Department of Chemical and Biomolecular Engineering, Rice University, Houston, TX 77005, USA*

† Electronic supplementary information (ESI) available. See DOI: 10.1039/d0ee03567j

Introduction

Hydrogen peroxide (H_2O_2) is a versatile chemical that is widely used in chemical synthesis, cosmetics and medicine, pulp and paper production, and wastewater treatment.[1–5] At present, industrial synthesis of H_2O_2 proceeds through the hydrogenation of anthraquinone (AQ) with H_2 and the subsequent oxidation by O_2 in an organic solvent is a multi-step process

that requires a high energy input and noble metal catalysts.[6,7] In addition, it generates hazardous solvent wastes. Direct synthesis of H_2O_2 from H_2 and O_2 has emerged as an alternative process for low-cost and decentralized synthesis.[8–10] However, the low production rate of H_2O_2, the need for subsequent H_2O_2 purification, and safety concerns related to handling potentially explosive H_2 and O_2 gases pose major challenges for practical use. Therefore, novel environmentally benign and facile methods for H_2O_2 synthesis are needed.

Photoelectrochemical (PEC) synthesis of H_2O_2 *via* water oxidation and dioxygen reduction has received growing attention as an alternative green method.[11–14] Reductive and oxidative pathways for the PEC synthesis of H_2O_2 are based on the oxygen reduction reaction (ORR) *via* two-electron transfer (*i.e.*, O_2/H_2O_2, E° = 0.68 V)[15] and the water oxidation reaction (WOR) *via* two-electron transfer (*i.e.*, H_2O_2/H_2O, E° = 1.76 V).[16,17] The selective two-electron reduction of O_2 to produce H_2O_2 is being intensively investigated by using various photocatalysts that include metal oxides and carbon nitrides.[18–21] Based on these fundamental redox reactions, extensive studies have focused on the development of various catalysts to improve selectivity and efficiency, and have demonstrated the capability of the PEC system for H_2O_2 synthesis *via* photoanodic, cathodic, or dual photoanodic–cathodic processes.[12,22–26] However, the concentration of H_2O_2 synthesized using the PEC system has been limited to a few milli-molar, which impedes its practical implementation. The additional challenges that the PEC system faces for practical applications are the separation and purification of the synthesized H_2O_2. The PEC systems presently used for H_2O_2 synthesis usually need high concentrations of electrolytes (summarized in Table S1, ESI†). However, no PEC study has demonstrated the production of electrolyte-free H_2O_2 solution due to the difficulty of separating H_2O_2 from electrolytes. Therefore, an additional process to purify the as-synthesized H_2O_2 from electrolytes in the PEC cell is needed.

Recently, direct synthesis of pure H_2O_2 solution has been achieved using a solid polymer electrolyte (SPE) electrolysis cell.[27–31] The utilization of SPE enables the synthesis of pure H_2O_2 without any ionic impurities. Wang's group recently reported the direct electrochemical synthesis of pure H_2O_2 solution *via* independent electrochemical reaction of H_2 and O_2 streams, followed by the ionic recombination process leading to the production of H_2O_2.[32] The SPE layer placed between the anode and the cathode facilitates the recombination of H^+ and HO_2^- ions crossing from the anode and cathode compartments, respectively, and deionized (DI) water flowing into the SPE layer dissolves pure H_2O_2 formed by the recombination of H^+ and HO_2^- ions. In contrast, in the previous studies that employed SPE,[27–31] they used a catalyst-coated gas diffusion layer electrode to enable the direct oxidation of H_2 gas on the anode and achieved notably high H_2O_2 concentration of ~20 wt% and faradaic efficiencies (FEs) ~90%. This approach offers an attractive route for the synthesis of pure H_2O_2 solution.

Here, we applied the SPE design to a PEC system for the direct synthesis of pure (electrolyte-free) H_2O_2 solution from water and O_2 only (without H_2) under solar irradiation

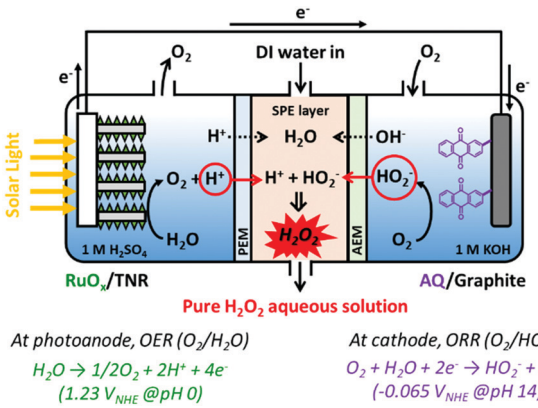

Scheme 1 Solar-driven synthesis of pure H_2O_2 aqueous solution using a photoelectrochemical cell with solid polymer electrolyte (SPE) in the absence of applied electrical bias.

(Scheme 1 and Fig. S1, ESI†). The RuO_x-deposited TiO_2 nanorod (RuO_x/TNR) photoanode initiates WOR to produce H^+ ions upon irradiation, and HO_2^- ions are produced on the AQ-anchored graphite rod (AQ/G) cathode *via* ORR. The SPE-containing middle compartment facilitates the selective transport of H^+ and HO_2^-, and DI water that flows into the middle compartment dissolves the *in situ* generated H_2O_2. By modifying both photoanode and cathode, continuous photosynthesis of H_2O_2 was achieved under a bias-free (0.0 V of cell voltage) condition over 100 h. The present study successfully achieved the highest concentration of pure H_2O_2 and the longest durability among all the reported PEC works of H_2O_2 synthesis (see Table S1, ESI†). Since this PEC system requires only water and O_2 (H_2 is not required unlike the electrochemical synthesis that requires H_2 gas[32]) with sunlight as the sole energy source, a sustainable and environmentally benign method is successfully demonstrated for the synthesis of H_2O_2.

Experimental

Fabrication of photoanodes and cathodes

TiO_2 nanorod (denoted as TNR) photoanodes were fabricated on fluorine-doped tin oxide substrates (FTO, Pilkington, 15 Ωsquare^{-1}) *via* a hydrothermal method.[33,34] Briefly, the two pieces of FTO slides (1 × 1 or 2 × 2 cm^2) were vertically placed while the conductive sides faced the wall in a Teflon-lined stainless steel autoclave (total 100 mL volume) containing 25 mL HCl (Aldrich, 37%), 1 mL titanium(IV) butoxide (Aldrich, 97%), and 25 mL deionized (DI) water (18.3 MΩ cm, Barnstead EASYpure RO system). The autoclave was placed in a pre-heated oven at 170 °C for 6 h, and then cooled to room temperature. The as-synthesized samples were rinsed with DI water and dried in air, followed by annealing at 550 °C for 1 h with a ramping rate of 10 °C min^{-1}. To synthesize RuO_x-deposited TNR (denoted as RuO_x/TNR) photoanodes, 10 μL cm^{-2} of $RuCl_3$ (10 mM, Aldrich, 99.98%) in ethanol (J. T. Baker, 99.9%) was drop-cast onto the as-annealed TNR samples. After drying at room temperature in air for 30 min, the samples were

immersed in 0.1 M KOH solution for 1 min to form oxides. $FeNiO_x$ and CoO_x-deposited TNR (denoted as $FeNiO_x$/TNR and CoO_x/TNR) photoanodes were fabricated using the same preparation procedure as that of RuO_x/TNR except for the metal precursors. The solutions containing either 4 mM $FeCl_2$ + 6 mM $NiCl_2$ or 10 mM $CoCl_2$ in ethanol were prepared for $FeNiO_x$ and CoO_x, respectively, prior to the deposition process. The graphite rod (Aldrich, diameter 6 mm, 99.995%) was directly employed as a cathode substrate without further purification. AQ-anchored graphite rod (denoted as AQ/G) cathodes were synthesized *via* a simple solution immersion process. Typically, a graphite rod (denoted as G) was immersed in ethanol containing anthraquinone-2-carboxylic acid (AQ-2-COOH, 3 mM, Aldrich, 98%) for 24 h, and dried at room temperature in air.

(Photo)Electrochemical measurements and analysis

The (photo)electrochemical performance of the RuO_x/TNR and AQ/G electrodes was measured in a typical three-electrode system using an electrochemical workstation (VersaSTAT 3-400, Princeton Applied Research) with a two-compartment cell separated by a proton exchange membrane (Nafion Membrane N117) containing 1 M H_2SO_4 and 1 M KOH in an anode compartment and a cathode compartment, respectively. A Pt foil and a Ag/AgCl electrode were used as the counter and reference electrodes, respectively, and, when needed, a Hg/HgO electrode was also used as an alternative reference electrode. The Ag/AgCl electrode was immersed in the anode compartment. Cyclic voltammograms (CVs) of bare and modified graphite rods were obtained in the range of 0.06 to −1.06 V (*vs.* Hg/HgO) at a scan rate of 50 mV s^{-1} in the dark. The solutions were purged with Ar (99.9%) or O_2 (99.9%) gas for at least 30 min prior to and during the measurements. A constant potential (−0.14, −0.24, −0.34, −0.44, or −0.54 V *vs.* Ag/AgCl) was applied to the bare G or AQ/G electrode, while measuring the amounts of synthesized H_2O_2 in the cathode compartment. Linear sweep voltammograms (LSVs) of bare and modified TNR samples were obtained in the range of −0.20 to +1.80 V (*vs.* Ag/AgCl) at a scan rate of 50 mV s^{-1} in the dark and under simulated sunlight (AM 1.5G, 100 mW cm^{-2}). A constant potential (+0.80, +1.30, and +1.80 V *vs.* Ag/AgCl) was applied to bare TNR or RuO_x/TNR electrode, while measuring O_2 evolution in the headspace of the anode compartment. The solution was purged with Ar gas for 30 min prior to the reaction.

For PEC synthesis of H_2O_2, a three-compartment-stack system was adopted to combine WOR and ORR. The stacked cell was composed of an anode compartment with photoanode (*i.e.*, TNR or RuO_x/TNR) in 1 M H_2SO_4 solution, a middle compartment filled with polystyrene crosslinked with divinylbenzene microspheres (Aldrich, 6.0–10.0 μm size) as a solid polymer electrolyte through which DI water flowed, and a cathode compartment with a cathode (*i.e.*, bare G or AQ/G) in 1 M KOH solution purged with O_2 gas. A proton exchange membrane (PEM, Nafion Membrane N117) and an anion exchange membrane (AEM, AMI-7001S, Membrane International) were placed between the anode and the middle compartments and between the middle and the cathode compartments, respectively (Scheme 1). The Ag/AgCl electrode was immersed in the anode compartment. The LSVs of the photoanode-SPE-cathode unit with various configurations (*i.e.*, TNR‖SPE‖G, TNR‖SPE‖AQ/G, RuO_x/TNR‖SPE‖G, and RuO_x/TNR‖SPE‖AQ/G) were obtained in the range of −0.20 to +1.80 V (*vs.* Ag/AgCl) at a scan rate of 50 mV s^{-1} under simulated sunlight (AM 1.5G, 100 mW cm^{-2}). A constant potential (+0.80, +1.30, or +1.80 V *vs.* Ag/AgCl) was applied to the TNR or RuO_x/TNR electrode, while measuring H_2O_2 in the middle compartment. If necessary, a two-electrode system without the Ag/AgCl reference electrode was also adopted in the same three-compartment-stack system by applying 0.0 V of cell voltage between the photoanode and cathode electrodes.

For electrochemical rotating ring-disk electrode (RRDE) voltammograms, a Pt ring/glassy carbon disk working electrode (ring OD 7 mm/ID 5 mm, disk ID 4 mm, ALS Co., no. 012613), a Pt wire counter electrode, and a Ag/AgCl reference electrode were placed in a single cell containing 0.1 M KOH (pH 13). The bare G and AQ/G samples were ground in a mortar to obtain fine powder, and 30 mg of powder and 12 μL of Nafion solution (Aldrich, 5 wt% in a mixture of lower aliphatic alcohols and water (40%)) were dissolved and well dispersed in 1 mL of ethanol by sonication for 30 min. A 5 μL aliquot of the solution mixture was drop-casted onto the glassy carbon disk and dried at room temperature for 10 min. The drop-casting process was repeated up to 3 times. The LSVs of bare G and AQ/G were obtained in the range of 0.0 to −0.6 V (*vs.* Ag/AgCl) with a scan rate of 10 mV s^{-1} using an electrochemical workstation with bi-potentiostat mode. The solution was pre-purged with O_2 gas for at least 30 min prior to and during the measurements. The rotation speed was varied from 100 to 1600 revolutions per minute (rpm) using a rotating ring disk electrode rotator (RRDE-3A, ALS Co., Ltd).

The amounts of the synthesized H_2O_2 and HO_2^- were quantified using the iodometric titration method. For H_2O_2, 0.50 mL aliquot of the sample was mixed with 1.50 mL of DI water, 0.75 mL of $C_8H_5KO_4$ (0.1 M potassium biphthalate, Alfa Aesar, 98%) solution, and 0.75 mL of KI (0.4 M, Aldrich, 99.5%) solution containing NaOH (0.06 M) and $(NH_4)_2MoO_4$ (10^{-4} M, Aldrich, 99%). After vigorous stirring for 2 min, the absorbance was measured at 372 nm using a UV/Visible spectrophotometer (Libra S22, Biochrom). For HO_2^-, 0.5 mL aliquot of the sample was mixed with 0.10 mL HCl (1 M), 1.4 mL of DI water, 0.75 mL of $C_8H_5KO_4$ solution, and 0.75 mL of KI solution containing NaOH and $(NH_4)_2MoO_4$. The faradaic efficiency (FE) for H_2O_2 or HO_2^- synthesis was calculated using the following: $FE = (2Fn/Q_{ph}) \times 100\%$, where F is the Faraday constant, n is the measured amount of evolved H_2O_2 or HO_2^- (mol), and Q_{ph} is the integrated photocharge.

While applying a constant potential to the working electrode, the amount of evolved O_2 was quantified in the headspace of the working electrode compartment using a gas chromatograph (GC, HP6890A) equipped with a thermal conductivity detector (TCD) and a 5 Å molecular sieve column. Prior to irradiation, the solution in the working electrode compartment was purged with Ar gas for 30 min to remove dissolved oxygen.

During the measurements, 100 μL of gas sample was intermittently withdrawn from the working electrode headspace using a gastight glass syringe (Hamilton 81030). The FE for O_2 evolution was calculated using the following: FE = $(4Fn/Q_{ph}) \times 100\%$, where F is the Faraday constant, n is the measured amount of evolved O_2 (mol), and Q_{ph} is the integrated photocharge.

Surface characterization

The surface morphologies of TNR and RuO_x/TNR were analyzed using high resolution field emission scanning electron microscopy (FE-SEM, JOEL JSM-7800F PRIME) with dual energy dispersive X-ray spectroscopy (EDS) at National Institute for Nanomaterials Technology (Pohang, Korea). X-ray diffraction (XRD) patterns of the samples were measured using Cu Kα radiation (RIGAKU D MAX 2500). X-ray photoelectron spectroscopy (XPS) was analyzed using monochromated Al Kα radiation as the X-ray source (1486.6 eV) at Korea Basic Science Institute (Busan Center, Korea). All XPS peak binding energies were referenced against the adventitious C 1s peak. The surface functional groups of the samples were analyzed using attenuated total reflectance Fourier transform infrared spectroscopy (ATR-FTIR; Thermo Scientific iS50) using a ZeSe crystal with a scan number of 100. The bare G and AQ/G powder samples were obtained by grinding in a mortar.

Results and discussion

Highly selective 2-electron reduction of O_2 on anthraquinone-anchored graphite rod

The Fourier transform infrared (FT-IR) spectra of bare graphite rod (G) and AQ-anchored graphite rod (AQ/G) samples revealed the presence of anthraquinone in the AQ/G sample (Fig. 1a). The IR spectrum of the AQ/G sample exhibited the apparent peaks of AQ at 696, 1267, 1666, and 1701 cm^{-1}, indicating the presence of AQ on the graphite rod that was anchored using a simple solution immersion process, while the bare graphite rod exhibited no peaks of AQ. The electrochemical (EC) performance of G and AQ/G samples was investigated using cyclic voltammetry (CVs) in 1 M KOH (pH ~ 13.6) solution purged with Ar or O_2 gas (Fig. 1b). The graphite rod was used as the cathode substrate since it exhibited superior EC activity when anchored with AQ among different carbon-based substrates (Fig. S2, ESI†). The CV scan of AQ/G samples under Ar gas exhibited typical peaks of the two-electron redox process of anthraquinone/anthrahydroquinone (AQ/AHQ), corroborating the presence of AQ molecules on the graphite rod, while bare G did not exhibit such peaks.[12,35,36]

Upon O_2 purging, the AQ/G samples exhibited significant reduction currents with an onset potential of +0.8 V_{RHE} for ORR, while bare G exhibited lower ORR currents. The FE for EC H_2O_2 synthesis in each potential was calculated based on the amount of HO_2^- synthesized on G and AQ/G, which was

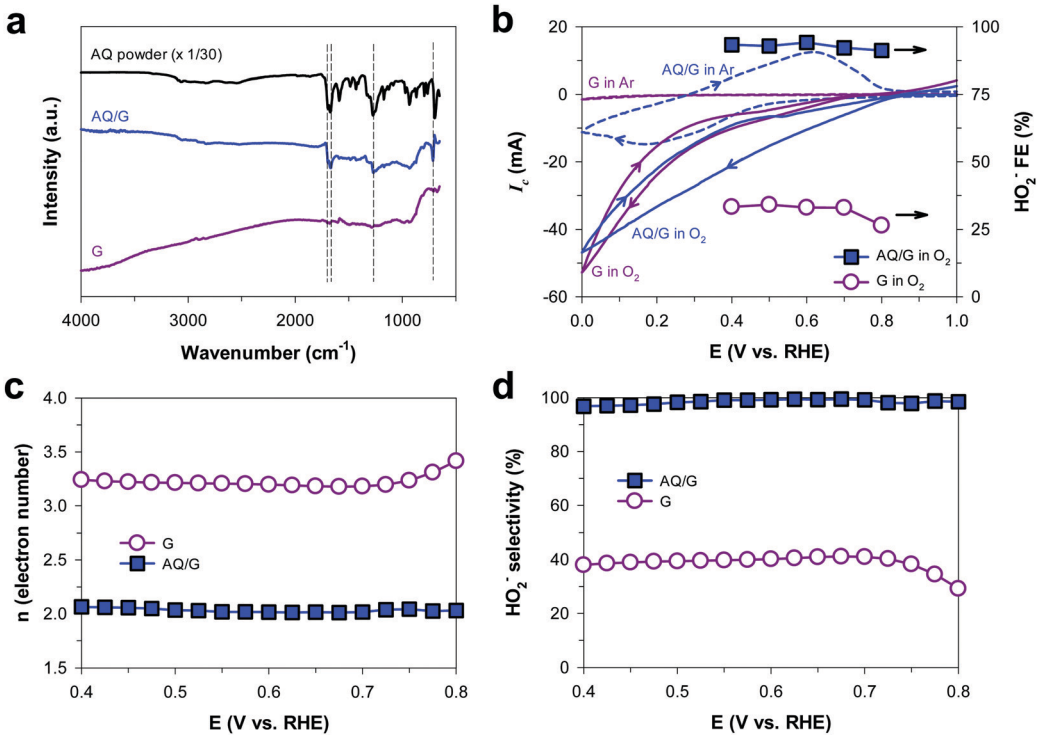

Fig. 1 (a) FTIR spectra of bare graphite rod (G) and anthraquinone-modified graphite rod (AQ/G). For comparison, the spectrum of anthraquinone (AQ) powder is also shown. (b) Cyclic voltammograms (CVs) of bare G and AQ/G under Ar and O_2 in 1 M KOH and faradaic efficiencies (FEs) for HO_2^- production. (c) The number of electrons transferred to the cathode and (d) the selectivity for HO_2^- with bare G and AQ/G at different potentials, which were obtained from RRDE experiments. See Fig. S3 (ESI†) for RRDE disk and ring currents recorded.

measured by sampling the solution in the cathode compartment. The ORR leads to the generation of H_2O_2 and HO_2^- as products under acidic and alkaline conditions, respectively.[37,38] Since the EC performance of the G and AQ/G electrodes was investigated in 1 M KOH, the actual form of product in this study should be HO_2^- ($pK_a(H_2O_2)$ = 11.75). The reactions were performed at each constant potential bias for 1 h; the FE values for the synthesis of HO_2^- on AQ/G reached 90–95% over the tested potential range, while that on bare G exhibited FE values in the range of 25–40%, which indicates the superior role of AQ in the 2-electron ORR process.

The EC activity of AQ in the ORR process was further investigated using the rotating ring-disk electrode (RRDE) experiments. The RRDE technique is a well-established method to determine ORR activities, and it can estimate the electron transfer number (n) and HO_2^- selectivity (%) based on RRDE current–potential curves and equations with ring and disk currents (see Fig. S3 for more details, ESI†).[39,40] AQ/G samples exhibited n = 2.0 and near 100% of HO_2^- selectivity across a potential range, while bare G samples exhibited $n \sim 3.3$ and ~40% of HO_2^- selectivity (Fig. 1c and d). This clearly indicates that AQ anchored on the graphite rod plays a critical role in the highly selective 2-electron ORR toward HO_2^- synthesis, which is in good agreement with the high FE of HO_2^- synthesis on AQ/G electrode (Fig. 1b).

Water photooxidation on RuO_x-deposited TiO_2 nanorod that provides electrons and protons

The TiO_2 nanorod (TNR) synthesized *via* the hydrothermal method exhibited typical rectangular bunched morphology with ~50 nm width and ~2.3 μm length (Fig. 2a and b). The deposition of RuO_x on TNR (RuO_x/TNR) induced a slight change in morphology, resulting in the deposition of needle-like structures on the nanorod arrays (Fig. 2c). The XPS spectra of Ru 3d and Ru 3p for the RuO_x/TNR samples confirmed the presence of Ru element on TNR, while bare TNR exhibited no apparent peaks in the spectra (Fig. 3a and b). The XPS spectra of Ti 2p for the RuO_x/TNR samples exhibited a slight shift to higher binding energy compared to that of bare TNR, indicating the interaction between RuO_x and TiO_2 (Fig. 3b). The XPS O 1s bands for TNR and RuO_x/TNR also exhibited a similar shift in binding energy between the two samples, showing 0.61 and 0.60 eV for Ti $2p_{1/2}$ and O 1s, respectively (Fig. 3c). XRD patterns of TNR and RuO_x/TNR samples exhibited identical rutile TiO_2 peaks with predominant (101) plane at 36.8° (Fig. 3d), indicating that the formation of RuO_x catalysts on TNT did not affect the crystalline phase. In addition, there were no additional peaks associated with the deposition of RuO_x on TNR, which implies the amorphous nature of the RuO_x phase. The loading of RuO_x catalysts had a minimal effect on the optical properties of TNR (Fig. 3e).

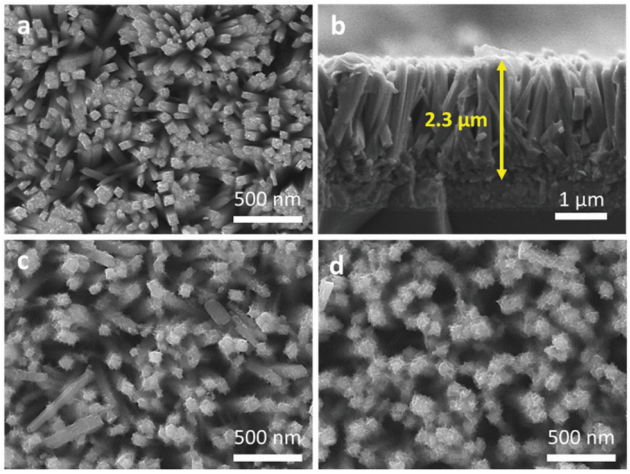

Fig. 2 SEM images of bare TNR from (a) top view and (b) cross-sectional view, (c) fresh RuO_x-deposited TNR (RuO_x/TNR), and (d) used RuO_x/TNR over 100 h.

The PEC performance of bare TNR and RuO_x/TNR samples was investigated using linear sweep voltammetry (LSVs) in 1 M H_2SO_4 (pH ~ 0.15) solution purged with Ar under solar simulating conditions (AM 1.5G, 100 mW cm^{-2}) (Fig. 4a). The LSVs of RuO_x/TNR exhibited superior performance for WOR to that of TNR. The deposition of RuO_x on TNR induced both a negative shift (−0.1 V_{RHE}) in the onset potential and a higher photocurrent. The operation parameters under the bias-free conditions can be predicted by comparing the LSVs of the photoanode and the cathode, which were obtained separately in the three-electrode system. The intersection point of LSV curves of the photoanode and the cathode indicates the ideal bias-free photocurrent when combining the two electrodes.[41,42] The photoanodic current of RuO_x/TNR and the cathodic current of AQ/G under O_2 saturation intersect at 1.23 mA and 0.81 V, indicating that this electrode configuration can operate without an external potential bias. The FEs for O_2 evolution *via* WOR were much higher for RuO_x/TNR than for bare TNR (Fig. 4b). In addition, CoO_x and $FeNiO_x$, which are well-known water oxidation catalysts, were also prepared and tested as co-catalysts on TNR.[43–45] CoO_x/TNR and $FeNiO_x$/TNR exhibited a higher photocurrent and a higher FE (O_2) than bare TNR, but lower than RuO_x/TNR.

PEC synthesis of pure H_2O_2 solution

To produce pure aqueous H_2O_2 solution that does not contain electrolytes, a PEC system that employed solid polymer electrolyte (SPE) was designed (Scheme 1). The PEC performance of various combined configurations using the photoanodes (TNR and RuO_x/TNR) and the cathodes (G and AQ/G) was investigated using LSVs under solar simulating irradiation. The anode and cathode compartments contained 1 M H_2SO_4 and 1 M KOH purged with O_2, respectively, with the SPE layer in a middle compartment through which DI water flowed. The electrode configuration using RuO_x/TNR and AQ/G exhibited the highest photocurrent generation (Fig. 5a), which is consistent with the enhanced (photo)electrochemical performance of the RuO_x/TNR photoanode and the AQ/G cathode. This enhanced PEC performance of the RuO_x/TNR‖SPE‖AQ/G configuration should be attributed to the combined action of WOR and ORR on the photoanode and the cathode, which produces H^+ and HO_2^- ions, respectively.

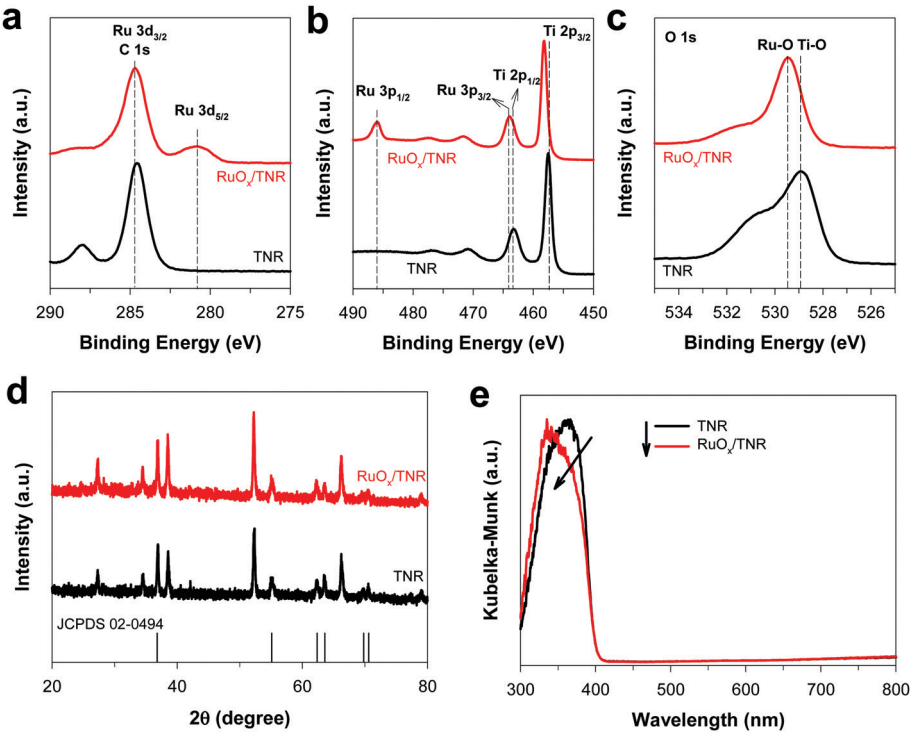

Fig. 3 XPS spectra of (a) C 1s and Ru 3d, (b) Ti 2p and Ru 3p, and (c) O 1s for TNR and RuO_x/TNR. (d) XRD patterns of TNR and RuO_x/TNR. The reference peaks represent rutile TiO_2. (e) UV-vis diffusion reflectance absorption spectra of bare TNR and RuO_x/TNR. All spectra were expressed in Kubelka–Munk (K.M.) unit (K.M. = $(1 - R^2)/2R$, where R represents the reflectance of the sample).

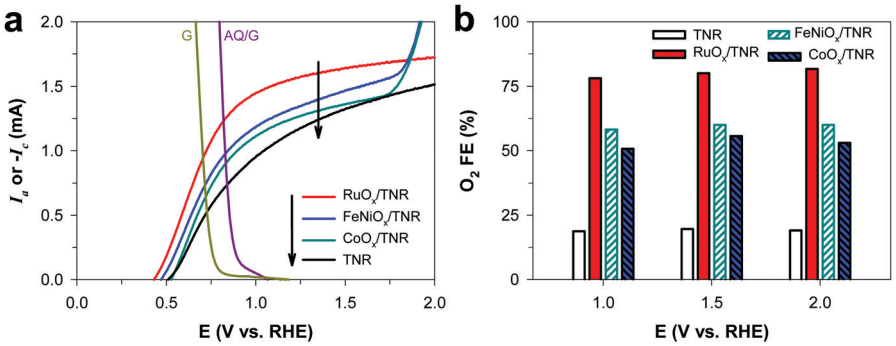

Fig. 4 (a) Linear sweep voltammograms (LSVs) of bare TNR, RuO_x/TNR, $FeNiO_x$/TNR, and CoO_x/TNR in 1 M H_2SO_4. For comparison, cathodic currents of bare G and AQ/G under O_2 saturation (from Fig. 1b) are also shown. (b) The faradaic efficiencies (FEs) for O_2 evolution at various potential bias. The reaction was performed for 1 h. All experiments were performed under solar simulating conditions (AM 1.5G, 100 mW cm^{-2}).

These ions generated on the electrode surface transport into the middle compartment through the proton exchange membrane and the anion exchange membrane, respectively, and subsequently recombine to form H_2O_2. The resulting H_2O_2 is then dissolved in the flowing DI water. The SPE layer can shuttle ions between the photoanode and the cathode in the solid phase instead of using liquid electrolyte. As SPE is the ion-conducting layer, its presence facilitates the ion transport and the recombination between H^+ and HO_2^- ions in the middle compartment, which help in maintaining the neutral pH in the middle compartment. Without the SPE layer in the middle compartment, the PEC cell would suffer from high resistance between the photoanode and the cathode and slow ionic transportation. In addition, as SPE is insoluble in water and has a porous structure, pure H_2O_2 can be formed and collected by water flow through SPE. The concentration of pure aqueous H_2O_2 (electrolyte-free) collected in the PEC-SPE system was measured and compared among various electrode configurations (Fig. 5b). The RuO_x/TNR‖SPE‖AQ/G configuration yielded not only the highest concentration of H_2O_2 ($\sim$0.8 mM), but also the highest FE ($\sim$90%) in the tested potential range. These results clearly indicate that the enhanced performance of RuO_x/TNR for the production of H^+ by WOR and AQ/G for the production of HO_2^- by ORR leads to the high-yield synthesis of H_2O_2.

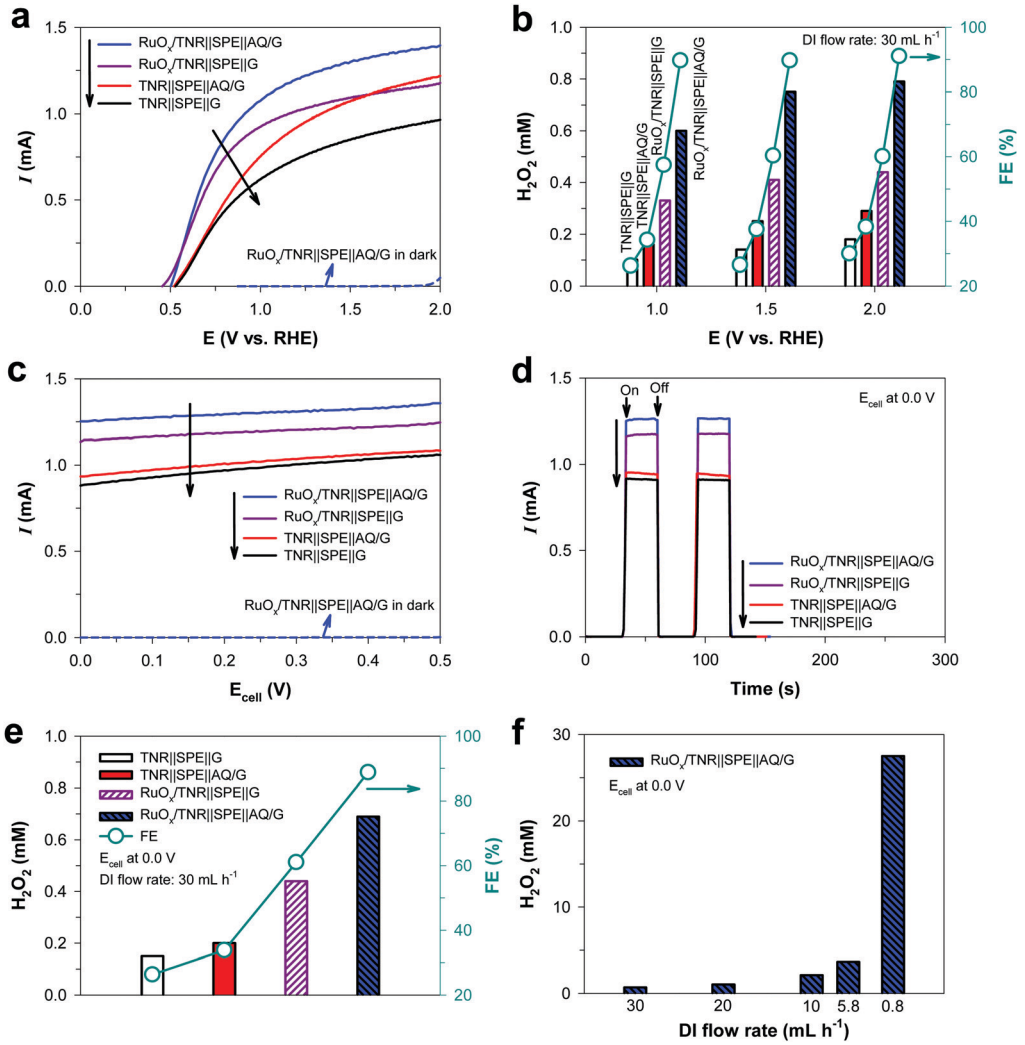

Fig. 5 (a) Linear sweep voltammograms (LSVs) and (b) *in situ* generated H_2O_2 concentration (mM) of the PEC cells with solid polymer electrolyte (SPE) in various electrode configurations (three-electrode system) at different potential bias. The reaction at each potential was performed for 1 h with DI water flow rate of 30 mL h^{-1}. (c) LSVs of the SPE-PEC cells in a two-electrode system. (d) The photocurrent–time profiles at E_{cell} = 0.0 V. (e) H_2O_2 concentration (mM) generated with various electrode configurations at E_{cell} = 0.0 V for 1 h. (f) H_2O_2 concentration (mM) obtained in the RuO_x/TNR‖SPE‖AQ/G cell (at E_{cell} = 0.0 V for 1 h) under different DI water flow rates. All experiments were performed under solar simulating condition (AM 1.5G, 100 mW cm^{-2}). For comparison, the electrochemical activities of the RuO_x/TNR‖SPE‖AQ/G configuration in three-electrode and two-electrode systems are also shown in (a) and (c), respectively.

The PEC performance of the configuration using RuO_x/TNR and AQ/G electrodes was also investigated without the SPE layer in the middle compartment (Fig. S4, ESI†). The configuration without SPE in the middle compartment, in which only DI water flows through, exhibited unstable photocurrents. In addition, it was observed that electrolytes in the anode and cathode compartments leaked into the middle compartment without SPE through the membranes, resulting in the change in pH in the anode and cathode compartments. On the other hand, the neutral pH of the middle compartment solution could be maintained in the presence of SPE, while it changed to alkaline pH without SPE. This clearly indicates that the presence of the SPE layer could inhibit the transportation of undesired cation (K^+) and anion (SO_4^{2-}) into the middle compartment. Although OH^- gets transported through the anion exchange membrane along with HO_2^-, the OH^- ions immediately recombine with H^+ ions (to form H_2O) which are transported into the SPE layer from the anode compartment (1 M H_2SO_4) through the proton exchange membrane. As a result, the middle compartment where pure H_2O_2 solution was generated maintained the neutral pH condition during the continuous PEC reaction and continuously generated a concentrated H_2O_2 solution during the 100 h irradiation (see Fig. 6c).

The PEC performance of the configurations was further investigated using LSVs under irradiation in a two-electrode system (Fig. 5c). The potential was directly applied between the photoanode and the cathode, which is indicated as the cell voltage (E_{cell}). The RuO_x/TNR‖SPE‖AQ/G configuration also exhibited the highest photocurrents and photocurrents of

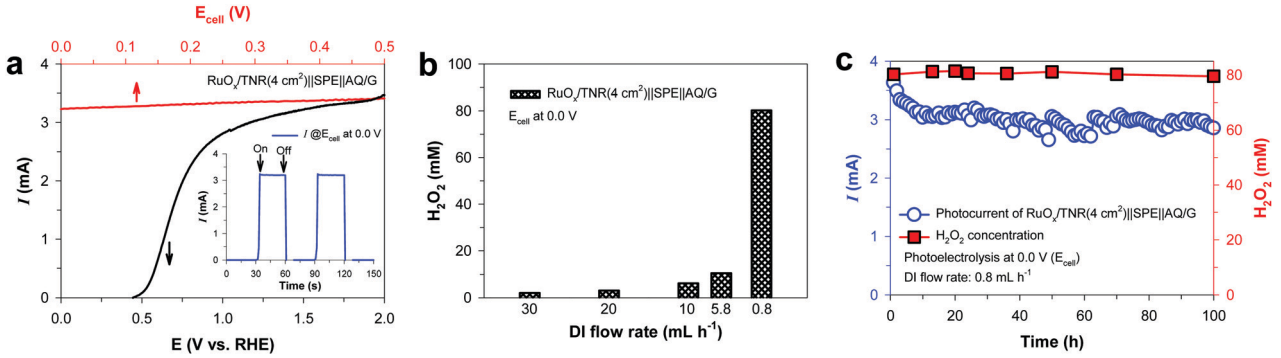

Fig. 6 (a) Linear sweep voltammograms (LSVs) of the RuO_x/TNR‖SPE‖AQ/G configuration with a larger photoanode (4 cm^2 instead of 1 cm^2) in the three-electrode (black curve) and the two-electrode (red curve) systems. The inset shows photocurrent generation in the two-electrode system at E_{cell} = 0.0 V. (b) H_2O_2 concentration (mM) obtained in the RuO_x/TNR‖SPE‖AQ/G cell (at E_{cell} = 0.0 V for 1 h) under different DI water flow rates. (c) Durability test for the continuous synthesis of H_2O_2 at E_{cell} = 0.0 V over 100 h. All experiments were performed under solar simulating condition (AM 1.5G, 100 mW cm^{-2}).

1.23 mA were generated for RuO_x/TNR‖SPE‖AQ/G configuration even under the bias-free conditions (at E_{cell} = 0.0 V) (Fig. 5d) as it is shown in Fig. 4a as an operating point under the bias-free conditions. On the other hand, there is a chemical bias (~0.8 V) developed between the photoanode and the cathode due to the pH difference (pH 0 *vs.* pH 14) of the electrolyte solutions even in the absence of the applied electrical bias, which could be a factor contributing to the high PEC efficiency under electrical bias-free conditions. Synthesis of H_2O_2 could also be achieved under the bias-free conditions, and the RuO_x/TNR‖SPE‖AQ/G configuration generated H_2O_2 at a concentration of ~0.7 mM with an FE of ~90% (Fig. 5e). The concentration of *in situ* generated H_2O_2 solution could be controlled by changing the DI water flow rate in the middle compartment (Fig. 5f). Using the optimized configuration (*i.e.*, RuO_x/TNR‖SPE‖AQ/G), a maximum H_2O_2 concentration of ~30 mM was obtained at a DI flow rate of 0.8 mL h^{-1}.

A higher concentration level of H_2O_2 production could be achieved by using a larger photoanode (RuO_x/TNR with the surface area of 4 cm^2 instead of 1 cm^2) in the RuO_x/TNR‖SPE‖AQ/G configuration. The LSVs of the larger photoanode show that higher photocurrents could be obtained in both three-electrode and two-electrode systems (Fig. 6a). Production of H_2O_2 under the bias-free conditions could reach up to ~80 mM in 1 h irradiation by varying the DI water flow rate (Fig. 6b). The durability of the PEC cell was also investigated under the bias-free conditions (Fig. 6c). A stable photocurrent of ~3 mA was maintained under a prolonged irradiation over 100 h while continuously producing ~80 mM level of H_2O_2 under the DI flow rate of 0.8 mL h^{-1}. This clearly demonstrates that the production of pure H_2O_2 solution could successfully be obtained in an engineered PEC system using sunlight as the sole energy source and the scale-up of the photoanode should produce higher concentrations (beyond mM level) of H_2O_2 solution. The surface morphology of the photoanode after 100 h of operation exhibited no sign of erosion (Fig. 2d).

Conclusions

Previous studies of PEC systems for the synthesis of H_2O_2 have employed a batch cell in which the *in situ* produced H_2O_2 is present with undesired ions (*e.g.*, electrolytes), and further energy-intensive purification processes that may generate hazardous waste streams are needed to obtain high purity H_2O_2. Here, we designed a new PEC system with a three-compartment cell which consists of a photoanode compartment, a cathode compartment, and an intervening SPE compartment. The three-compartment cell initiates water oxidation to produce H^+ in the photoanode (RuO_x/TNR) compartment and oxygen reduction to generate HO_2^- in the cathode (AQ/G) compartment, and subsequently recombines H^+ and HO_2^- to form pure (electrolyte-free) H_2O_2 in the SPE compartment with the continuous flow of DI water. H^+ and HO_2^- ions are selectively transported into the SPE compartment through PEM and AEM, respectively. The DI water flows through the middle SPE compartment and dissolves the as-formed H_2O_2 to obtain pure H_2O_2 solution.

The PEC synthesis of pure H_2O_2 solution could be successfully achieved under external bias-free (0.0 V of cell voltage) conditions using sunlight as the sole external energy source, while producing a continuous flow of ~80 mM H_2O_2 solution over 100 h with no sign of photocurrent decline. The performance of the present PEC system achieved a significantly higher H_2O_2 concentration than those reported in previous studies (Table S1, ESI†). Note that all the previous studies reported H_2O_2 solutions mixed with electrolytes, while this work generated pure H_2O_2 solution. However, the solar-to-H_2O_2 conversion efficiency of the three-compartment PEC cell was only ~0.42%, which is mainly ascribed to the low solar absorption capacity of TNR. With the employment of visible light-absorbing photoanodes, there should be more room for further improvement. More studies with the optimized (photo)electrode combination are needed for better performance. In addition, although this system can produce pure H_2O_2 solution under bias-free conditions, the

three-compartment PEC system also suffers from resistance from stacking for high current collection, low ionic conductivity of SPE, and instability of membranes for long-term operation. Further studies should attempt to overcome these drawbacks.

Conflicts of interest

There are no conflicts to declare.

Acknowledgements

This research was financially supported by the Leading Researcher Program (NRF-2020R1A3B2079953), which was funded by the Korea government (MSIT) through the National Research Foundation of Korea (NRF). Partial support was provided by the NSF ERC on Nanotechnology-Enabled Water Treatment (EEC-1449500). The authors would like to thank Dr Hyunwoong Park (Kyungpook National University) and Sunghun Kim for technical support with the photoelectrochemical cell and membranes.

References

1 G. Strukul, *Catalytic oxidations with hydrogen peroxide as oxidant*, Springer Science & Business Media, 2013.
2 N. Agarwal, S. J. Freakley, R. U. McVicker, S. M. Althahban, N. Dimitratos, Q. He, D. J. Morgan, R. L. Jenkins, D. J. Willock and S. H. Taylor, *Science*, 2017, **358**, 223–227.
3 R. Hage and A. Lienke, *Angew. Chem., Int. Ed.*, 2006, **45**, 206–222.
4 A. D. Bokare and W. Choi, *J. Hazard. Mater.*, 2014, **275**, 121–135.
5 H. Kim, J. Lim, S. Lee, H.-H. Kim, C. Lee, J. Lee and W. Choi, *Environ. Sci. Technol.*, 2019, **53**, 2918–2925.
6 J. M. Campos-Martin, G. Blanco-Brieva and J. L. Fierro, *Angew. Chem., Int. Ed.*, 2006, **45**, 6962–6984.
7 Q. Chen, *Chem. Eng. Process.*, 2008, **47**, 787–792.
8 R. J. Lewis and G. J. Hutchings, *ChemCatChem*, 2019, **11**, 298–308.
9 S. J. Freakley, Q. He, J. H. Harrhy, L. Lu, D. A. Crole, D. J. Morgan, E. N. Ntainjua, J. K. Edwards, A. F. Carley and A. Y. Borisevich, *Science*, 2016, **351**, 965–968.
10 J. K. Edwards, E. Ntainjua, A. F. Carley, A. A. Herzing, C. J. Kiely and G. J. Hutchings, *Angew. Chem., Int. Ed.*, 2009, **48**, 8512–8515.
11 S. Hu, *Sustainable Energy Fuels*, 2019, **3**, 101–114.
12 T. H. Jeon, H. Kim, H.-I. Kim and W. Choi, *Energy Environ. Sci.*, 2020, **13**, 1730–1742.
13 K. Fuku, Y. Miyase, Y. Miseki, T. Funaki, T. Gunji and K. Sayama, *Chem. – Asian J.*, 2017, **12**, 1111–1119.
14 K. Zhang, J. Liu, L. Wang, B. Jin, X. Yang, S. Zhang and J. H. Park, *J. Am. Chem. Soc.*, 2020, **142**, 8641–8648.
15 D. S. Choi, H. Lee, F. Tieves, Y. W. Lee, E. J. Son, W. Zhang, B. Shin, F. Hollmann and C. B. Park, *ACS Catal.*, 2019, **9**, 10562–10566.
16 J. Liu, Y. Zou, B. Jin, K. Zhang and J. H. Park, *ACS Energy Lett.*, 2019, **4**, 3018–3027.
17 X. Shi, S. Siahrostami, G.-L. Li, Y. Zhang, P. Chakthranont, F. Studt, T. F. Jaramillo, X. Zheng and J. K. Nørskov, *Nat. Commun.*, 2017, **8**, 701.
18 P. Zhang, Y. W. Tong, Y. Liu, J. J. M. Vequizo, H. W. Sun, C. Yang, A. Yamakata, F. T. Fan, W. Lin, X. C. Wang and W. Choi, *Angew. Chem., Int. Ed.*, 2020, **59**, 16209–16217.
19 P. Zhang, D. Sun, A. Cho, S. Weon, S. Lee, J. Lee, J. W. Han, D.-P. Kim and W. Choi, *Nat. Commun.*, 2019, **10**, 940.
20 G.-h. Moon, M. Fujitsuka, S. Kim, T. Majima, X. Wang and W. Choi, *ACS Catal.*, 2017, **7**, 2886–2895.
21 G.-h. Moon, W. Kim, A. D. Bokare, N.-e. Sung and W. Choi, *Energy Environ. Sci.*, 2014, **7**, 4023–4028.
22 X. Shi, Y. Zhang, S. Siahrostami and X. Zheng, *Adv. Energy Mater.*, 2018, **8**, 1801158.
23 F. Ye, T. Wang, X. Quan, H. Yu and S. Chen, *Chem. Eng. J.*, 2020, **389**, 123427.
24 M. Ko, Y. J. Sa, J. Woo, T. V. T. Nguyen, J. H. Kim, D. Oh, P. Sharma, J. Ryu, T. J. Shin and S. H. Joo, *Nat. Commun.*, 2019, **10**, 5123.
25 W. Fan, B. Zhang, X. Wang, W. Ma, D. Li, Z. Wang, M. Dupuis, J. Shi, S. Liao and C. Li, *Energy Environ. Sci.*, 2020, **13**, 238–245.
26 K. Mase, M. Yoneda, Y. Yamada and S. Fukuzumi, *Nat. Commun.*, 2016, **7**, 11470.
27 I. Yamanaka, S. Tazawa, T. Murayama, T. Iwasaki and S. Takenaka, *ChemSusChem*, 2010, **3**, 59–62.
28 T. Murayama and I. Yamanaka, *J. Phys. Chem. C*, 2011, **115**, 5792–5799.
29 I. Yamanaka and T. Murayama, *Angew. Chem., Int. Ed.*, 2008, **120**, 1926–1928.
30 S. J. You, J. Y. Wang, N. Q. Ren, X. H. Wang and J. N. Zhang, *ChemSusChem*, 2010, **3**, 334–338.
31 J. Choi, S. H. Hwang, J. Jang and J. Yoon, *Electrochem. Commun.*, 2013, **30**, 95–98.
32 C. Xia, Y. Xia, P. Zhu, L. Fan and H. Wang, *Science*, 2019, **366**, 226–231.
33 B. Liu and E. S. Aydil, *J. Am. Chem. Soc.*, 2009, **131**, 3985–3990.
34 S. Kim, G. Piao, D. S. Han, H. K. Shon and H. Park, *Energy Environ. Sci.*, 2018, **11**, 344–353.
35 A. Sarapuu, K. Vaik, D. J. Schiffrin and K. Tammeveski, *J. Electroanal. Chem.*, 2003, **541**, 23–29.
36 G. Pognon, T. Brousse, L. Demarconnay and D. Bélanger, *J. Power Sources*, 2011, **196**, 4117–4122.
37 T. Yano, D. Tryk, K. Hashimoto and A. Fujishima, *J. Electrochem. Soc.*, 1998, **145**, 1870.
38 J. Zhang and L. Dai, *ACS Catal.*, 2015, **5**, 7244–7253.
39 R. Zhou, Y. Zheng, M. Jaroniec and S.-Z. Qiao, *ACS Catal.*, 2016, **6**, 4720–4728.

40 K. Jiang, S. Back, A. J. Akey, C. Xia, Y. Hu, W. Liang, D. Schaak, E. Stavitski, J. K. Nørskov and S. Siahrostami, *Nat. Commun.*, 2019, **10**, 3997.
41 Y. Surendranath, D. K. Bediako and D. G. Nocera, *Proc. Natl. Acad. Sci. U. S. A.*, 2012, **109**, 15617–15621.
42 J. H. Kim, D. Hansora, P. Sharma, J.-W. Jang and J. S. Lee, *Chem. Soc. Rev.*, 2019, **48**, 1908–1971.
43 X. Deng and H. Tüysüz, *ACS Catal.*, 2014, **4**, 3701–3714.
44 K. Fominykh, P. Chernev, I. Zaharieva, J. Sicklinger, G. Stefanic, M. Döblinger, A. Müller, A. Pokharel, S. Böcklein and C. Scheu, *ACS Nano*, 2015, **9**, 5180–5188.
45 R. D. Smith, M. S. Prévot, R. D. Fagan, Z. Zhang, P. A. Sedach, M. K. J. Siu, S. Trudel and C. P. Berlinguette, *Science*, 2013, **340**, 60–63.

